

# Transverse magnetic field and chiral-nonchiral transition in vortex states for nearly $B \parallel ab$ in chiral $p$ -wave superconductors

Masahiro Ishihara, Yuujirou Amano, Masanori Ichioka,\* and Kazushige Machida  
*Department of Physics, Okayama University, Okayama 700-8530, JAPAN*  
 (Dated: June 4, 2018)

On the basis of Eilenberger theory, we study the vortex state when a magnetic field is applied nearly parallel to the  $ab$  plane in a chiral  $p$ -wave superconductor with a large anisotropy ratio of  $ab$  and  $c$ , as in  $\text{Sr}_2\text{RuO}_4$ . We quantitatively estimate the field dependence of the pair potential, magnetization, and flux line lattice form factor, and study the transition from the chiral  $p_-$  state at low fields to the nonchiral  $p_y$  state at high fields. Even for exactly parallel fields to the  $ab$  plane, transverse fields exist in the chiral state. The chiral-nonchiral transition disappears when the magnetic field orientation is tilted within  $1^\circ$  from the  $ab$  plane. This may be a reason why the experimental detection of this transition is difficult.

PACS numbers: 74.25.Uv, 74.70.Pq, 74.20.Rp, 74.25.Ha

## I. INTRODUCTION

Chiral  $p$ -wave superconductivity attracts much attention as one of representative topological superconductors.<sup>1</sup> The chiral  $p$ -wave superconductivity with the pairing function  $p_\pm (= p_x \pm ip_y)$  is a possible pairing state, when the  $p$ -wave pairing interaction works instead of the conventional  $s$ -wave pairing. The pairing function  $p_\pm$  breaks time-reversal symmetry, inducing spontaneous magnetic fields observed by  $\mu\text{SR}$  experiments.<sup>2</sup> We also expect that Majorana states are accommodated at vortices and surfaces in chiral  $p$ -wave superconductors.<sup>3,4</sup> This type of pairing is realized in the A phase of superfluid  $^3\text{He}$ , and is a candidate for the superconducting phase of  $\text{Sr}_2\text{RuO}_4$ .<sup>5,6</sup> However, there remain mysteries for the pairing symmetry of  $\text{Sr}_2\text{RuO}_4$ , since we have not observed some typical phenomena expected in chiral  $p$ -wave superconductors. For example, when a magnetic field  $\bar{\mathbf{B}}$  is applied in the orientation  $\bar{\mathbf{B}} \parallel ab$ , theoretically we expect the transition from the chiral  $p_\pm$ -wave state at low fields to the nonchiral  $p_y$ -wave state (when  $\bar{\mathbf{B}} \parallel y$ ) at high fields.<sup>7,8</sup> That is, at low fields, the free energy of the chiral  $p_\pm$ -wave state is lower than that of nonchiral  $p_x$ - or  $p_y$ -wave states, because the latter nonchiral states have vertical line nodes. On the other hand, the nonchiral state is realized at high fields, because the upper critical field  $H_{c2}$  of the  $p_y$  state is higher than that of the chiral  $p_\pm$ -wave state when  $\bar{\mathbf{B}} \parallel y$ . While the chiral-nonchiral transition was suggested by experiments of the magnetization curve,<sup>9</sup> this transition was not observed in other experimental methods.<sup>6,10,11</sup> There were discussions in that the double transition<sup>5,6,11</sup> near  $H_{c2}$  corresponds to the chiral-nonchiral transition.<sup>8</sup>

On the other hand, in superconductors with uniaxial anisotropy, transverse magnetic fields appear in the vortex state when the field orientation is tilted from the  $ab$  plane.<sup>12</sup> This transverse field is detected by the spinflip scattering of the small angle neutron scattering (SANS) in the vortex states, as demonstrated in  $\text{YBa}_2\text{Cu}_3\text{O}_{7-\delta}$ .<sup>13</sup> Recently, the spin flip SANS by the transverse field was reported in  $\text{Sr}_2\text{RuO}_4$ .<sup>14</sup> Therefore, the quantitative the-

oretical estimate of the transverse field is expected. It is also important to find new phenomena by the contribution of Cooper pair's angular momentum  $L_z/\hbar = \pm 1$  of the  $p_\pm$ -wave paring.

The purpose of this study is to establish quantitative theoretical estimations of the vortex structure in chiral  $p$ -wave superconductors when a magnetic field is applied to exactly  $\bar{\mathbf{B}} \parallel ab$ , and when the field orientation is slightly tilted from the  $ab$  plane. On the basis of Eilenberger theory by which we can quantitatively calculate the spatial structure and the physical quantities of the vortex states,<sup>15-18</sup> we will clarify behaviors of the chiral-nonchiral transition and the transverse field structure as a function of a magnetic field  $\bar{B}$ .

## II. FORMULATION BY EILENBERGER THEORY

As a model of the Fermi surface, we use a quasi-two dimensional Fermi surface with a rippled cylinder shape. The Fermi velocity is assumed to be  $\mathbf{v} = (v_a, v_b, v_c) \propto (\cos \phi, \sin \phi, \tilde{v}_z \sin p_c)$  at  $\mathbf{p} = (p_a, p_b, p_c) \propto (p_F \cos \phi, p_F \sin \phi, p_c)$  on the Fermi surface.<sup>16</sup> We consider a case  $\tilde{v}_z = 1/60$ , producing large anisotropy ratio of coherence lengths,  $\gamma \equiv \xi_c/\xi_b \sim \langle v_c^2 \rangle_{\mathbf{p}}^{1/2} / \langle v_b^2 \rangle_{\mathbf{p}}^{1/2} \sim 1/60$ ,<sup>14</sup> where  $\langle \dots \rangle_{\mathbf{p}}$  indicates an average over the Fermi surface. The magnetic field is tilted within  $1^\circ$  from the  $ab$  plane. Since we set the  $z$  axis to the vortex line direction, the coordinate  $(x, y, z)$  for the vortex structure is related to the crystal coordinate  $(a, b, c)$  as  $(x, y, z) = (a, b \cos \theta + c \sin \theta, c \cos \theta - b \sin \theta)$  with  $\theta = 90^\circ \sim 89^\circ$ .

In a chiral  $p$ -wave superconductor, the pair potential takes the form,

$$\Delta(\mathbf{p}, \mathbf{r}) = \Delta_+(\mathbf{r})\phi_+(\mathbf{p}) + \Delta_-(\mathbf{r})\phi_-(\mathbf{p}) \quad (1)$$

with the pairing functions  $\phi_\pm(\mathbf{p}) = (p_a \pm ip_b)/p_F = e^{\pm i\phi}$ .  $\Delta_\pm(\mathbf{r})$  describes the vortex structure as a function of  $\mathbf{r}$  (the center of mass coordinate of the pair). In our study,  $\Delta_-(\mathbf{r})$  is a main component and  $\Delta_+(\mathbf{r})$  is a passive

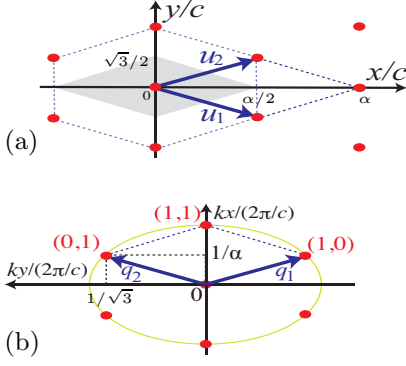


FIG. 1: (Color online) (a) Unit vectors  $\mathbf{u}_1$  and  $\mathbf{u}_2$  of the vortex lattice. Circles indicate the vortex centers. The gray region is a unit cell of our calculations. (b) Unit vectors  $\mathbf{q}_1$  and  $\mathbf{q}_2$  in the reciprocal space. Circles indicate the SANS spots  $(h, k)$ .

component induced around a vortex.<sup>15,19</sup> At a zero field,  $\Delta_+(\mathbf{r}) = 0$ . When we consider the  $p_x$ - and  $p_y$ -wave components, the pair potential is decomposed as  $\Delta(\mathbf{p}, \mathbf{r}) = \Delta_x(\mathbf{r})\phi_x(\mathbf{p}) + \Delta_y(\mathbf{r})\phi_y(\mathbf{p})$  with  $\phi_x(\mathbf{p}) = \sqrt{2}p_a = \sqrt{2}\cos\phi$  and  $\phi_y(\mathbf{p}) = \sqrt{2}p_b = \sqrt{2}\sin\phi$ .

Using the anisotropic ratio  $\Gamma_\theta \equiv \xi_y/\xi_x \sim \langle v_y^2 \rangle_{\mathbf{p}}^{1/2} / \langle v_x^2 \rangle_{\mathbf{p}}^{1/2} \sim (\cos^2\theta + \gamma^{-2}\sin^2\theta)^{-1/2}$ , we set the unit vectors of the vortex lattice as  $\mathbf{u}_1 = c(\alpha/2, -\sqrt{3}/2)$  and  $\mathbf{u}_2 = c(\alpha/2, \sqrt{3}/2)$  with  $c^2 = 2\phi_0/(\sqrt{3}\alpha\bar{B})$  and  $\alpha = 3\Gamma_\theta$ ,<sup>16</sup> as shown in Fig. 1(a).  $\phi_0$  is the flux quantum, and  $\bar{B}$  is the flux density. As shown in Fig. 1(b), the unit vectors in the reciprocal space are given by  $\mathbf{q}_1 = (2\pi/c)(1/\alpha, -1/\sqrt{3})$  and  $\mathbf{q}_2 = (2\pi/c)(1/\alpha, 1/\sqrt{3})$ , where spots of the SANS appear.

Quasiclassical Green's functions  $f(\omega_n, \mathbf{p}, \mathbf{r})$ ,  $f^\dagger(\omega_n, \mathbf{p}, \mathbf{r})$ ,  $g(\omega_n, \mathbf{p}, \mathbf{r})$  in the vortex lattice states are obtained by solving the Riccati equation, which is derived from the Eilenberger equation

$$\begin{aligned} \{\omega_n + \hat{\mathbf{v}} \cdot (\nabla + i\mathbf{A})\} f &= \Delta g, \\ \{\omega_n - \hat{\mathbf{v}} \cdot (\nabla - i\mathbf{A})\} f^\dagger &= \Delta^* g. \end{aligned} \quad (2)$$

in the clean limit, with a normalization condition  $g = (1 - ff^\dagger)^{1/2}$  and the Matsubara frequency  $\omega_n$ .<sup>15-18</sup> That is, we calculate the spatial structure of  $g$  without using Pesch's approximation.<sup>8,20</sup> The normalized Fermi velocity is  $\hat{\mathbf{v}} = \mathbf{v}/v_F$  with  $v_F = \langle \mathbf{v}^2 \rangle_{\mathbf{p}}^{1/2}$ . We have scaled the length, temperature, magnetic field, and energies in units of  $\xi_0$ ,  $T_c$ ,  $B_0$ , and  $\pi k_B T_c$ , respectively, where  $\xi_0 = \hbar v_F / 2\pi k_B T_c$ ,  $B_0 = \phi_0 / 2\pi \xi_0^2$ . The vector potential  $\mathbf{A} = \frac{1}{2}\bar{\mathbf{B}} \times \mathbf{r} + \mathbf{a}(\mathbf{r})$  is related to the internal field as  $\mathbf{B}(\mathbf{r}) = \nabla \times \mathbf{A} = (B_x(\mathbf{r}), B_y(\mathbf{r}), B_z(\mathbf{r}))$  with  $\bar{\mathbf{B}} = (0, 0, \bar{B})$ ,  $B_z(\mathbf{r}) = \bar{B} + b_z(\mathbf{r})$  and  $(B_x, B_y, b_z) = \nabla \times \mathbf{a}$ . The spatial averages of  $B_x$ ,  $B_y$ , and  $b_z$  are zero.<sup>14</sup>

We calculate  $\Delta(\mathbf{p}, \mathbf{r})$  by the gap equation

$$\Delta_\pm(\mathbf{r}) = \lambda_0 2T \sum_{\omega_n > 0}^{\omega_c} \langle \phi_\pm^*(\mathbf{p}) f \rangle_{\mathbf{p}}, \quad (3)$$

where  $\lambda_0 = N_0 g_0$  is the dimensionless  $p$ -wave pairing interaction in the low-energy band  $|\omega_n| \leq \omega_c$ , defined by the cutoff energy  $\omega_c$  as  $1/\lambda_0 = \ln T + 2T \sum_{\omega_n > 0}^{\omega_c} \omega_n^{-1}$ . We carry out calculations using the cutoff  $\omega_c = 20k_B T_c$ . The current equation to obtain  $\mathbf{A}$  is given by

$$\mathbf{j}(\mathbf{r}) = \nabla \times (\nabla \times \mathbf{A}) = -\kappa^{-2} 2T \sum_{\omega_n > 0} \langle \hat{\mathbf{v}} \text{Im} g \rangle_{\mathbf{p}}. \quad (4)$$

The Ginzburg-Landau (GL) parameter  $\kappa$  is the ratio of the penetration depth to coherence length for  $\bar{\mathbf{B}} \parallel c$ , and set to be  $\kappa = 2.7$  appropriate to  $\text{Sr}_2\text{RuO}_4$ .<sup>5</sup> The case of effective GL parameter  $\kappa_\theta \sim \kappa \Gamma_\theta$  for a field orientation  $\theta$  is reproduced by the anisotropy of  $\hat{\mathbf{v}}$  in Eq. (4). Iterating calculations of Eqs. (2)-(4) at  $T = 0.5T_c$ , we obtain self-consistent solutions of  $\Delta_\pm(\mathbf{r})$ ,  $\mathbf{A}(\mathbf{r})$ , and quasiclassical Green's functions.

### III. EXACTLY PARALLEL FIELD TO THE BASAL PLANE

First, we study the vortex states for exactly  $\bar{\mathbf{B}} \parallel ab$  ( $\theta = 90^\circ$ ). In Fig. 2, we show the calculated spatial structures within a unit cell of the vortex lattice at low and high fields. The main component  $\Delta_-(\mathbf{r})$  has a winding 1 of the phase at the vortex center, where the amplitude  $|\Delta_-(\mathbf{r})|$  in Fig. 2(a) is suppressed. At low fields, the vortex core is localized at the center. At high fields the vortex core contribution becomes important in the properties of the vortex states, since the inter-vortex distances become shorter with increasing fields. As a property of chiral  $p$ -wave superconductors, the opposite chiral component  $\Delta_+(\mathbf{r})$  also appears where the main chiral component  $\Delta_-(\mathbf{r})$  has spatial modulations around vortex cores.<sup>15,19</sup> The amplitude of the induced component  $|\Delta_+(\mathbf{r})|$  is presented in Fig. 2(b). It appears locally around the vortex core at a low field  $\bar{B} = 2$ . With increasing fields, since the inter-vortex distances become shorter,  $\Delta_+(\mathbf{r})$  of neighbor vortex cores overlap with each other, as shown in panels for  $\bar{B} = 8$  and 16. With further increasing  $\bar{B}$ , the amplitude of  $\Delta_+(\mathbf{r})$  is reduced to  $|\Delta_+(\mathbf{r})| = |\Delta_-(\mathbf{r})|$ , as shown in a panel for  $\bar{B} = 20$  in Fig. 2(b). This indicates disappearance of  $\Delta_x(\mathbf{r})$  by the chiral-nonchiral transition from the chiral  $p_-$ -wave state to the nonchiral  $p_y$ -wave state.

The  $z$ -component of the internal field,  $B_z(\mathbf{r})$ , has a conventional spatial structure of the vortex lattice also for  $\bar{\mathbf{B}} \parallel ab$  in chiral  $p$ -wave superconductors, if the length is re-scaled by the effective coherence length in each direction. As shown in Fig. 2(c),  $B_z(\mathbf{r})$  has a peak at a vortex center, and decreases as a function of radius from the center. We note that the transverse components  $B_x(\mathbf{r})$  and  $B_y(\mathbf{r})$  appear even when exactly  $\bar{\mathbf{B}} \parallel ab$  in the chiral  $p_-$  state at low fields. This is unconventional behavior due to the contribution of the internal angular momentum  $L_z$  of the chiral pairing function. The transverse components vanish in nonchiral  $p_y$  states at high fields.

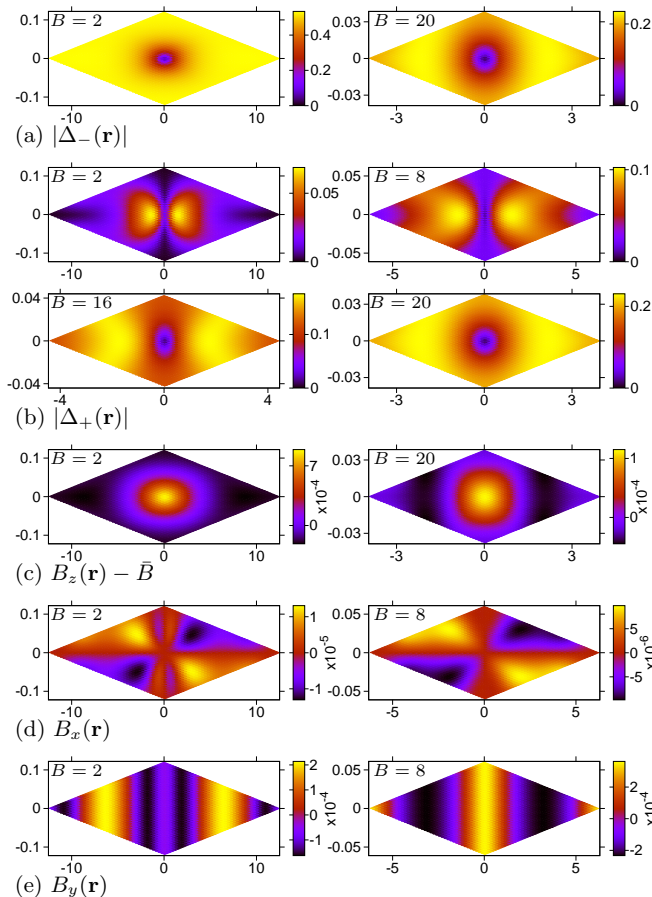


FIG. 2: (Color online) Density plots of the pair potential and the internal magnetic field within a unit cell [gray region in Fig. 1(a)] when  $\theta = 90^\circ$ . (a) Main  $p_-$  component of the pair potential,  $|\Delta_-(\mathbf{r})|$ , at  $\bar{B} = 2$  and 20. (b) Passive  $p_+$ -wave component  $|\Delta_+(\mathbf{r})|$  at  $\bar{B} = 2, 8, 16$ , and 20. (c)  $B_z(\mathbf{r}) - \bar{B}$  at  $\bar{B} = 2$  and 20. (d)  $B_x(\mathbf{r})$  at  $\bar{B} = 2$  and 8. (e)  $B_y(\mathbf{r})$  at  $\bar{B} = 2$  and 8.

To see the behaviors of the chiral-nonchiral transition, we plot the amplitudes of each component of the pair potential as a function of  $\bar{B}$  in Fig. 3(a). With increasing  $\bar{B}$ , the  $p_-$  wave component decreases and the  $p_+$  wave component increases. After the chiral-nonchiral transition at  $B > B^* \sim 18$ , the amplitudes of  $p_+$  and  $p_-$  are the same. If we see the pair potential in the decomposition of  $p_x$  and  $p_y$ , with increasing  $\bar{B}$ , the  $p_y$  component decreases toward zero at  $H_{c2}$  and the  $p_x$  component decreases toward zero at  $B^*$ .  $\Delta_x = 0$  at  $\bar{B} > B^*$  by the chiral-nonchiral transition. In Fig. 3(a), we also show the case of conventional  $s$ -wave pairing. Compared with the case of conventional  $s$ -wave pairing,  $H_{c2}$  is enhanced when the pairing function has a horizontal line node relative to the field direction.<sup>21</sup>

To discuss the  $\bar{B}$ -dependence of the internal field dis-

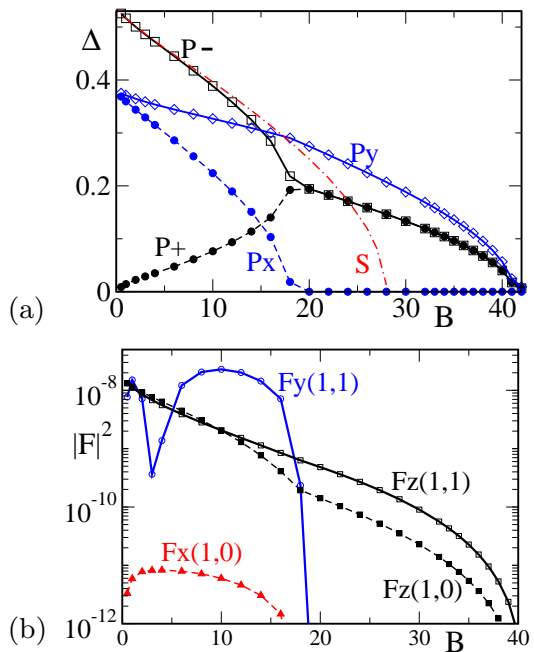


FIG. 3: (Color online) (a)  $\bar{B}$ -dependence of  $p_-$ ,  $p_+$ ,  $p_x$ , and  $p_y$  wave components of the pair potential when  $\theta = 90^\circ$ . Spatial averaged values of  $|\Delta_-|$ ,  $|\Delta_+|$ ,  $|\Delta_x|$ , and  $|\Delta_y|$  are presented. We also show the  $s$ -wave case for comparison. (b)  $\bar{B}$ -dependence of the FLL form factors when  $\theta = 90^\circ$ . We present  $|F_z(1,0)|^2$ ,  $|F_z(1,1)|^2$ ,  $|F_x(1,0)|^2$ , and  $|F_y(1,1)|^2$ . Other components  $|F_x(1,1)|^2$  and  $|F_y(1,0)|^2$  are less than  $10^{-12}$ . The vertical axis is log-scale.

tribution, we consider flux line lattice (FLL) form factors  $\mathbf{F}(\mathbf{q}_{h,k}) = (F_x(h,k), F_y(h,k), F_z(h,k))$  calculated as Fourier transformation of the internal field distribution,  $\mathbf{B}(\mathbf{r}) = \sum_{h,k} \mathbf{F}(\mathbf{q}_{h,k}) \exp(i\mathbf{q}_{h,k} \cdot \mathbf{r})$  with the wave vectors  $\mathbf{q}_{h,k} = h\mathbf{q}_1 + k\mathbf{q}_2$ .  $h$  and  $k$  are integers. The  $z$ -component  $|F_z(h,k)|^2$  from  $B_z(\mathbf{r})$  gives the intensity of spots in the conventional non-spinflip SANS experiments.<sup>22</sup> The transverse component,  $|F_{\text{tr}}(h,k)|^2 = |F_x(h,k)|^2 + |F_y(h,k)|^2$ , is accessible by the spin-flip SANS experiments.<sup>13,14</sup> In Fig. 3(b), we see exponential decays of  $|F_z(h,k)|^2$  as a function of  $\bar{B}$ , as in the conventional behavior of the vortex states, since we do not take care of the Pauli-paramagnetic effect.<sup>23</sup> The transverse components  $|F_x(1,0)|^2$  and  $|F_y(1,1)|^2$  appear only in the chiral states at  $\bar{B} < B^*$ . From the stripe pattern in the spatial structure of  $B_y(\mathbf{r})$  as in Fig. 2(e), the main spot of  $|F_y|^2$  is  $|F_y(1,1)|^2$ . The stripe pattern changes between  $\bar{B} = 2$  and 8. From the spatial pattern of  $B_x(\mathbf{r})$ , the main spot of  $|F_x(h,k)|^2$  is at  $(h,k) = (1,0)$ . The intensity of  $|F_x(1,0)|^2$  is much smaller than  $|F_y(1,1)|^2$ .

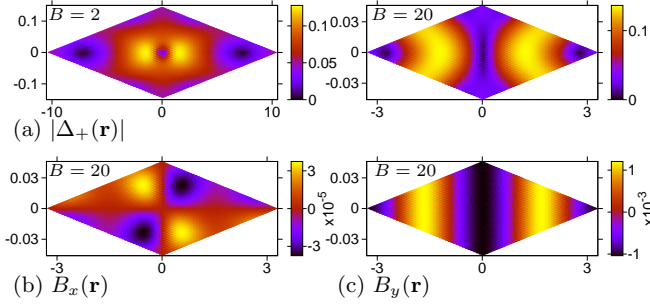


FIG. 4: (Color online) Density plots of the pair potential and the internal magnetic field within a unit cell when  $\theta = 89^\circ$ . (a)  $|\Delta_+(\mathbf{r})|$  at  $\bar{B} = 2$  and 20. (b)  $B_x(\mathbf{r})$  at  $\bar{B} = 20$ . (c)  $B_y(\mathbf{r})$  at  $\bar{B} = 20$ .

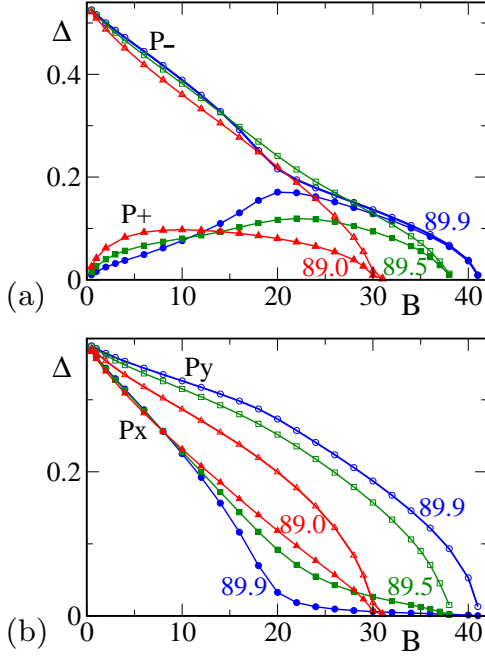


FIG. 5: (Color online)  $\bar{B}$ -dependence of each component of the pair potential in the vortex states, when the magnetic field is slightly tilted from the  $ab$  plane, i.e.,  $\theta = 89.9^\circ$ ,  $89.5^\circ$ , and  $89.0^\circ$ . (a) Spatial averaged  $|\Delta_-|$  and  $|\Delta_+|$ . (b) Spatial averaged  $|\Delta_x|$  and  $|\Delta_y|$ .

#### IV. FIELD ORIENTATION TILTED FROM THE BASAL PLANE

Next, we discuss the vortex states when the magnetic field is slightly tilted from the  $ab$  plane as  $89^\circ \leq \theta < 90^\circ$ . The vortex states in the  $p_-$ -wave domain, where  $\Delta_-(\mathbf{r})$  is the main component, has lower free energy than that in the  $p_+$ -wave domain where  $\Delta_+(\mathbf{r})$  is the main component. This is because the field orientation lifts up the degeneracy of the  $p_-$ - and  $p_+$ -wave domains.<sup>15,19</sup>

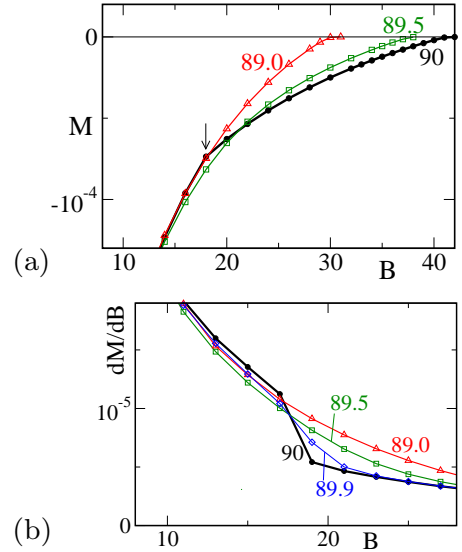


FIG. 6: (Color online) (a) Magnetization curve  $M(\bar{B})$  as a function of  $\bar{B}$  when the magnetic field is slightly tilted from the  $ab$  plane as  $89^\circ \leq \theta \leq 90^\circ$ . An arrow indicates  $B^*$ . (b) Derivative of the magnetization curve  $dM/d\bar{B}$  near  $B^*$  for  $89^\circ \leq \theta \leq 90^\circ$ .

Therefore, we study the stable  $p_-$ -wave domain case here.

When  $\theta = 89^\circ$ , around the vortex core of the main component  $\Delta_-(\mathbf{r})$ , the opposite chiral component  $\Delta_+(\mathbf{r})$  is also induced as presented in Fig. 4(a). There, the spatial pattern of  $|\Delta_-(\mathbf{r})|$  at  $\bar{B} = 2$  is similar to that of  $\bar{\mathbf{B}} \parallel c$  case,<sup>15</sup> rather than that of  $\bar{\mathbf{B}} \parallel ab$  in Fig. 2(b).  $|\Delta_+(\mathbf{r})|$  at a high field  $\bar{B} = 20$  keeps similar spatial structure to that of  $\bar{\mathbf{B}} \parallel ab$  case with  $\bar{B} = 8$  in Fig. 2(b). Thus  $|\Delta_+(\mathbf{r})| \neq |\Delta_-(\mathbf{r})|$  even at high fields, indicating that the nonchiral state with  $\Delta_x(\mathbf{r}) = 0$  does not realize. To see the disappearance of the chiral-nonchiral transition, we study the  $\bar{B}$ -dependence of each component of the pair potential for  $\theta = 89.9^\circ$ ,  $89.5^\circ$ , and  $89.0^\circ$ . As seen from the curve for  $89.9^\circ$  in Fig. 5(a), even if the field orientation is tilted by  $0.1^\circ$ , the chiral-nonchiral transition changes to a crossover behavior. At high fields, small differences between the  $p_-$  and  $p_+$  components still exist. Thus, in Fig. 5(b), a small amplitude of  $p_x$ -wave component survives up to  $H_{c2}$ . Further tilting the field orientation to  $89.5^\circ$  and  $89.0^\circ$ , the crossover behaviors are smeared, and we can not see the remnant of the chiral-nonchiral transition anymore. The amplitude of the  $p_x$ -wave component monotonically decreases toward  $H_{c2}$ .

The chiral-nonchiral transition is reflected by the magnetization curve,  $M = \bar{B} - H$  as a function of  $\bar{B}$ . From the selfconsistent solutions we obtain the relation of  $\bar{B}$  and the external field  $H$  as

$$H = \bar{B} + \left\langle (B_z(\mathbf{r}) - \bar{B})^2 \right\rangle_{\mathbf{r}} / \bar{B}$$

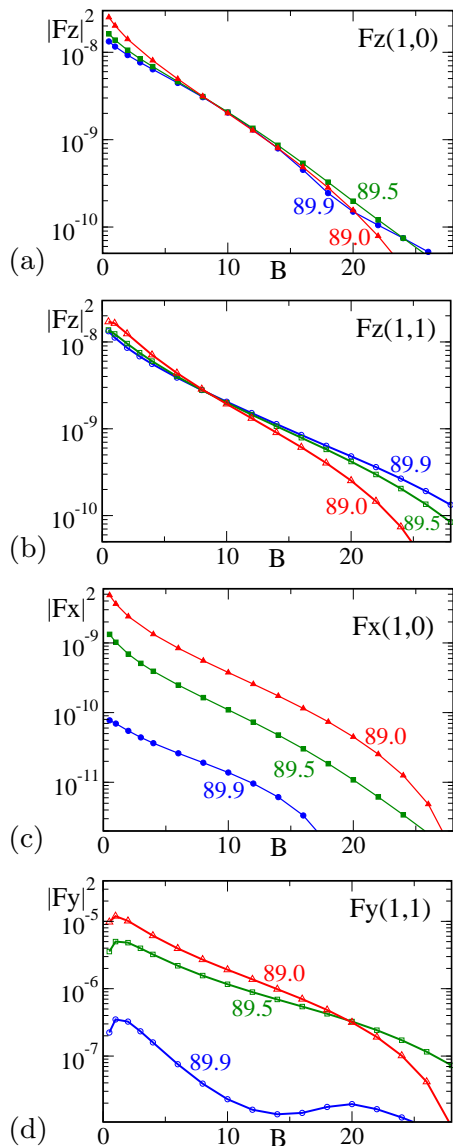


FIG. 7: (Color online)  $\bar{B}$ -dependence of the FLL form factors in the vortex states, when the magnetic field is slightly tilted from the  $ab$  plane, i.e.,  $\theta = 89.9^\circ$ ,  $89.5^\circ$ , and  $89.0^\circ$ . (a)  $|F_z(1,0)|^2$ . (b)  $|F_z(1,1)|^2$ . (c)  $|F_x(1,0)|^2$ . (d)  $|F_y(1,1)|^2$ . In (a)-(d), the vertical axis is log-scale.

$$+\frac{T}{\kappa^2 \bar{B}} \sum_{\omega_n > 0} \langle \langle \text{Re} \left\{ \frac{(f^\dagger \Delta + f \Delta^*) g}{2(g+1)} + \omega_n (g-1) \right\} \rangle_{\mathbf{p}} \rangle_{\mathbf{r}}, \quad (5)$$

which is derived by Doria-Gubernatis-Rainer scaling.<sup>24,25</sup>  $\langle \cdots \rangle_{\mathbf{r}}$  indicates a spatial average. In the magnetization curve in Fig. 6(a), we see a change of the slope at  $B^*$  for exactly  $\bar{\mathbf{B}} \parallel ab$  ( $\theta = 90^\circ$ ). This is clearly seen as a step at  $B^*$  in the plot of the derivative  $dM/dB$  in Fig. 6(b). However this behavior of second-order phase transition is smeared by tilting the field orientation within  $1^\circ$ . The step in  $dM/dB$  was suggested in the experimental observation of the magnetization curve.<sup>9</sup> However in other experimental methods such as specific heat and thermal conductivity,<sup>6,10,11</sup> the chiral-nonchiral transition has not

been observed yet. This may be because the experimental situation of exactly  $\bar{\mathbf{B}} \parallel ab$  is difficult to be realized. Our study shows that the chiral-nonchiral transition vanishes by tilting the field orientation within  $1^\circ$ .

In  $\text{Sr}_2\text{RuO}_4$ , when  $\bar{\mathbf{B}} \parallel ab$ ,  $H_{c2}$  is suppressed and changes to the first order phase transition.<sup>9,26,27</sup> Our simple formulation in this work does not include the mechanism for the suppression of  $H_{c2}$ , such as a Pauli-paramagnetic-like effect.<sup>28</sup> The study for this  $H_{c2}$  behavior belongs to future works.

Both in the  $\bar{B}$ -dependence of  $|F_z(10)|^2$  in Fig. 7(a) and  $|F_z(11)|^2$  in Fig. 7(b), with decreasing  $\theta$  from  $90^\circ$ ,  $|F_z|^2$  becomes larger at low fields, reflecting the decrease of the effective GL parameter  $\kappa_\theta$ . Roughly  $|F_z| \propto (\kappa_\theta)^{-1}$  from Eq. (4). On the other hand,  $|F_z|^2$  becomes smaller at high fields, because  $H_{c2}$  decreases by the decrease of  $\theta$ . As shown in Figs. 4(b)-(c),  $B_x(\mathbf{r})$  and  $B_y(\mathbf{r})$  have similar spatial structures until high fields to those of  $\bar{B} = 2$  and  $\theta = 90^\circ$  in Figs. 2(d)-(e). However, the amplitudes of  $B_x$  and  $B_y$  at  $\theta = 89^\circ$  are much larger than those at  $\theta = 90^\circ$ . Thus,  $|F_x(1,0)|^2$  in Fig. 7(c) and  $|F_y(1,1)|^2$  in Fig. 7(d) increase rapidly with decreasing  $\theta$  from  $90^\circ$ .  $|F_x(1,1)|^2$  and  $|F_y(1,0)|^2$  are less than  $10^{-12}$ .

When these form factors are compared with each other, the intensity of the spinflip SANS at  $\mathbf{q}_{1,1}$  from  $|F_y(1,1)|^2$  is much larger than that of the non-spinflip SANS intensity of  $|F_z(1,1)|^2$  and  $|F_z(1,0)|^2$ . On the other hand, very small intensity of the spinflip SANS at  $\mathbf{q}_{1,0}$  from  $|F_x(1,0)|^2$  is difficult to be observed. These correspond to the SANS experimental results on  $\text{Sr}_2\text{RuO}_4$ , where the spinflip SANS spot was observed only at  $\mathbf{q}_{1,1}$ .<sup>14</sup> Within the experimental resolution, the spin-flip SANS spot at  $\mathbf{q}_{1,0}$  and the non-spinflip SANS spots have not been observed yet. We note that similar behaviors of the transverse fields appear also in the nonchiral state including  $s$ -wave pairing, if  $\theta \neq 90^\circ$ . Thus, for  $\theta \neq 90^\circ$ , it is not easy that unique effects due to the chiral state are extracted from qualitative behaviors of the transverse fields

## V. SUMMARY

We studied the vortex states for nearly  $\bar{\mathbf{B}} \parallel ab$  in chiral  $p$ -wave superconductors on the basis of Eilenberger theory. The chiral-nonchiral transition at exactly  $\bar{\mathbf{B}} \parallel ab$  vanishes by tilting the magnetic field within  $1^\circ$ . We quantitatively estimated the FLL form factors including transverse fields, and showed that the spin-flip SANS intensity by the transverse fields has large intensity at  $(1,1)$ -spot. The transverse fields appear even when exactly  $\bar{\mathbf{B}} \parallel ab$ , as a unique effect of the chiral states. These theoretical results indicate the importance of careful studies about the vortex states for nearly  $\bar{\mathbf{B}} \parallel ab$ , to detect some natures of chiral  $p$ -wave superconductors or  $\text{Sr}_2\text{RuO}_4$ .

## Acknowledgments

We thank M. R. Eskildsen for fruitful discussions and information about their spin-flip SANS experiments.

- 
- \* ichioka@cc.okayama-u.ac.jp
- <sup>1</sup> C. Nayak, S.H. Simon, A. Stern, M. Freedman, and S. Das Sarma, *Rev. Mod. Phys.* **80**, 1083 (2008).
  - <sup>2</sup> G. M. Luke, Y. Fudamoto, K. M. Kojima, M. I. Larkin, J. Merrin, B. Nachumi, Y. J. Uemura, Y. Maeno, Z. Q. Mao, Y. Mori, H. Nakamura, and M. Sigrist, *Nature* **394**, 558 (1998).
  - <sup>3</sup> N. Read and D. Green, *Phys. Rev. B* **61**, 10267 (2000).
  - <sup>4</sup> D. A. Ivanov, *Phys. Rev. Lett.* **86**, 268 (2001).
  - <sup>5</sup> A. P. Mackenzie and Y. Maeno, *Rev. Mod. Phys.* **75**, 657 (2003).
  - <sup>6</sup> Y. Maeno, S. Kittaka, T. Nomura, S. Yonezawa, and K. Ishida, *J. Phys. Soc. Jpn.* **73**, 011009 (2011).
  - <sup>7</sup> D. F. Agterberg, *Phys. Rev. Lett.* **80**, 5184 (1998).
  - <sup>8</sup> R. P. Kaur, D. F. Agterberg, and H. Kusunose, *Phys. Rev. B* **72**, 144528 (2005).
  - <sup>9</sup> K. Tenya, S. Yasuda, M. Yokoyama, H. Amitsuka, K. Deguchi, and Y. Maeno, *J. Phys. Soc. Jpn.* **75**, 023702 (2006).
  - <sup>10</sup> K. Deguchi, Z. Q. Mao, and Y. Maeno, *J. Phys. Soc. Jpn.* **73**, 1313 (2004).
  - <sup>11</sup> H. Yaguchi, K. Deguchi, M. A. Tanatar, Y. Maeno, T. Ishiguro, *J. Phys. Chem. Solids* **63**, 1007 (2002).
  - <sup>12</sup> S. L. Thiemann, Z. Radović, and V. G. Kogan, *Phys. Rev. B* **39**, 11406 (1989).
  - <sup>13</sup> P. G. Kealey, D. Charalambous, E. M. Forgan, S. L. Lee, S. T. Johnson, P. Schleger, R. Cubitt, D. McK. Paul, C. M. Aegerter, S. Tajima, and A. Rykov, *Phys. Rev. B* **64**, 174501 (2001).
  - <sup>14</sup> C. Rastovski, C. D. Dewhurst, W. J. Gannon, D. C. Peets, H. Takatsu, Y. Maeno, M. Ichioka, K. Machida, and M. R. Eskildsen, arXiv:1302.4810.
  - <sup>15</sup> M. Ichioka and K. Machida, *Phys. Rev. B* **65**, 224517 (2002).
  - <sup>16</sup> M. Hiragi, K. M. Suzuki, M. Ichioka, and K. Machida, *J. Phys. Soc. Jpn.* **79**, 094709 (2010).
  - <sup>17</sup> U. Klein, *J. Low Temp. Phys.* **69**, 1 (1987).
  - <sup>18</sup> P. Miranović, M. Ichioka, and K. Machida *Phys. Rev. B* **70**, 104510 (2004).
  - <sup>19</sup> M. Ichioka, Y. Matsunaga, and K. Machida, *Phys. Rev. B* **71**, 172510 (2005).
  - <sup>20</sup> W. Pesch, *Z. Phys. B* **21**, 263 (1975).
  - <sup>21</sup> K. Scharnberg and R.A. Klemm, *Phys. Rev. B* **22**, 5233 (1980).
  - <sup>22</sup> T. M. Riseman, P. G. Kealey, E. M. Forgan, A. P. Mackenzie, L. M. Galvin, A. W. Tyler, S. L. Lee, C. Ager, D. M. Paul, C. M. Aegerter, R. Cubitt, Z. Q. Mao, T. Akima, and Y. Maeno, *Nature* **396**, 242 (1998); **404**, 629(E) (2000).
  - <sup>23</sup> M. Ichioka and K. Machida, *Phys. Rev. B* **76**, 064502 (2007); M. Ichioka, K. M. Suzuki, Y. Tsutsumi, and K. Machida, in *Superconductivity - Theory and Applications*, edited by A.M. Luiz (InTech, Croatia, 2011), Chap.10.
  - <sup>24</sup> K. Watanabe, T. Kita, and M. Arai, *Phys. Rev. B* **71**, 144515 (2005).
  - <sup>25</sup> M. M. Doria, J. E. Gubernatis, and D. Rainer, *Phys. Rev. B* **41**, 6335 (1990).
  - <sup>26</sup> S. Kittaka, T. Nakamura, Y. Aono, S. Yonezawa, K. Ishida, and Y. Maeno, *Phys. Rev. B* **80**, 174514 (2009).
  - <sup>27</sup> S. Yonezawa, T. Kajikawa, and Y. Maeno, *Phys. Rev. Lett.* **110**, 077003 (2013).
  - <sup>28</sup> K. Machida and M. Ichioka, *Phys. Rev. B* **77**, 184515 (2008).